*Canadian Mineralogist*
Vol. 27, pp. 509-523 (1989)

# EXTREME FACIES OF CONTACT METAMORPHISM DEVELOPED IN CALC-SILICATE XENOLITHS IN THE EASTERN BUSHVELD COMPLEX

THOMAS WALLMACH AND CHRISTOPHER J. HATTON
*Institute for Geological Research on the Bushveld Complex, University of Pretoria, 0002 Hillcrest, South Africa*

GILES T.R. DROOP
*Department of Geology, The University of Manchester, Manchester, England M13 9PL*

## ABSTRACT

Calc-silicate xenoliths in the eastern Bushveld Complex, South Africa, contain rare mineral parageneses that form only at extreme degrees of contact metamorphism. Certain of the observed mineral assemblages have not been described previously. A petrogenetic grid is proposed, which covers the highest known degrees of metamorphism occurring in the system $CaO–MgO–SiO_2–CO_2$. With increasing temperature, åkermanite, merwinite and periclase formed from irreversible decarbonation reactions in which calcite was a principal reactant. Forsterite exsolution in monticellite with an unusual optically positive sign indicate metamorphic temperatures higher than 1200°C, as does dehydroxylated barian phlogopite. Overburden load pressures of 0.6 – 1.6 kbars for the emplacement of the critical zone magma and 1.1 – 2.4 kbars for the marginal zone magma can be inferred from critical mineral parageneses. An overlap of these pressure estimates in the range of 1.1 to 1.6 kbars suggests that the Bushveld Complex was initially emplaced below a volcano-sedimentary pile 3 to 5 km thick. Critical mineral assemblages in xenoliths of the marginal zone indicate peak metamorphic temperatures lower than those recorded by xenoliths of the critical zone.

*Keywords:* contact metamorphism, calc-silicates, åkermanite, monticellite, merwinite, periclase, petrogenetic grid, *P–T* estimate, Bushveld Complex, South Africa.

## SOMMAIRE

Des enclaves de calc-silicates dans la partie orientale du complexe du Bushveld (Afrique du Sud) contiennent des assemblages peu communs qui témoignent d'un métamorphisme de contact intense. Certaines associations n'avaient jamais été signalés. Nous proposons un schéma pétrogénétique pour les facies extrêmes de métamorphisme dans le système $CaO–MgO–SiO_2–CO_2$. Avec une augmentation en température, åkermanite, merwinite et périclase cristallisent à la suite des réactions irréversibles de décarbonatation dans lesquelles la calcite était le réactif principal. La présence de lamelles d'exsolution de forsterite dans la monticellite dont le signe optique est positif, ainsi que de phlogopite baryfère déshydroxylée, indiquerait une température métamorphique en excès de 1200°C. Les assemblages définitifs indiquent une pression lithostatique entre 0.6 et 1.6 kbars pour la mise en place du magma qui a donné la zone critique du complexe, et entre 1.1 et 2.4 kbars pour la mise en place du magma de la zone marginale. Les valeurs communes, entre 1.1 et 1.6 kbars, concordent avec une mise en place du complexe du Bushveld en dessous d'un empilement volcano-sédimentaire de 3 à 5 km en épaisseur. Les assemblages définifs des enclaves de la zone marginale indiquent une température maximale de métamorphisme plus élevée que ceux des enclaves de la zone critique.

(Traduit par la Rédaction)

*Mots-clés:* métamorphisme de contact, calc-silicates, åkermanite, monticellite, merwinite, périclase, schéma pétrogénétique, géothermométrie, géobarométrie, complexe du Bushveld, Afrique du Sud.

## INTRODUCTION

The Bushveld Complex is known for its unique abundance of economically important mineralization. Considerable attention has been given to the possible mechanisms that may have led to the formation of the mineral deposits (*e.g.*, special issue of *Economic Geology*, v.80, 1985). In comparison, little work has been done on the evaluation of the depth of intrusion or the magma temperatures of the different Bushveld magmas. Calc-silicate xenoliths found in the Bushveld Complex display extremely rare and unusual minerals and mineral assemblages, which can be used as geothermometers and geobarometers. These calc-silicate xenoliths are situated in the marginal, critical and upper zones of the eastern Bushveld Complex.

Calc-silicate xenoliths in the Bushveld Complex have been described previously by several authors (Willemse & Bensch 1964, Page 1970, Joubert 1976, Mostert 1982). In a thorough petrological study of some of the minerals and mineral parageneses occurring in xenoliths found in the marginal zone of the Bushveld Complex (arrow A in Fig. 1), Willemse & Bensch (1964) described åkermanite–monticellite felses. Furthermore, they found intergrowths of wollastonite and monticellite, and of clinopyroxene and monticellite, the latter forming fine-grained symplectitic reaction rims separating coarse-grained olivine and åkermanite. Two retrograde reactions were proposed to explain these textures and parageneses:

1) åkermanite = monticellite + wollastonite;
2) 2 åkermanite + forsterite = 3 monticellite + diopside.

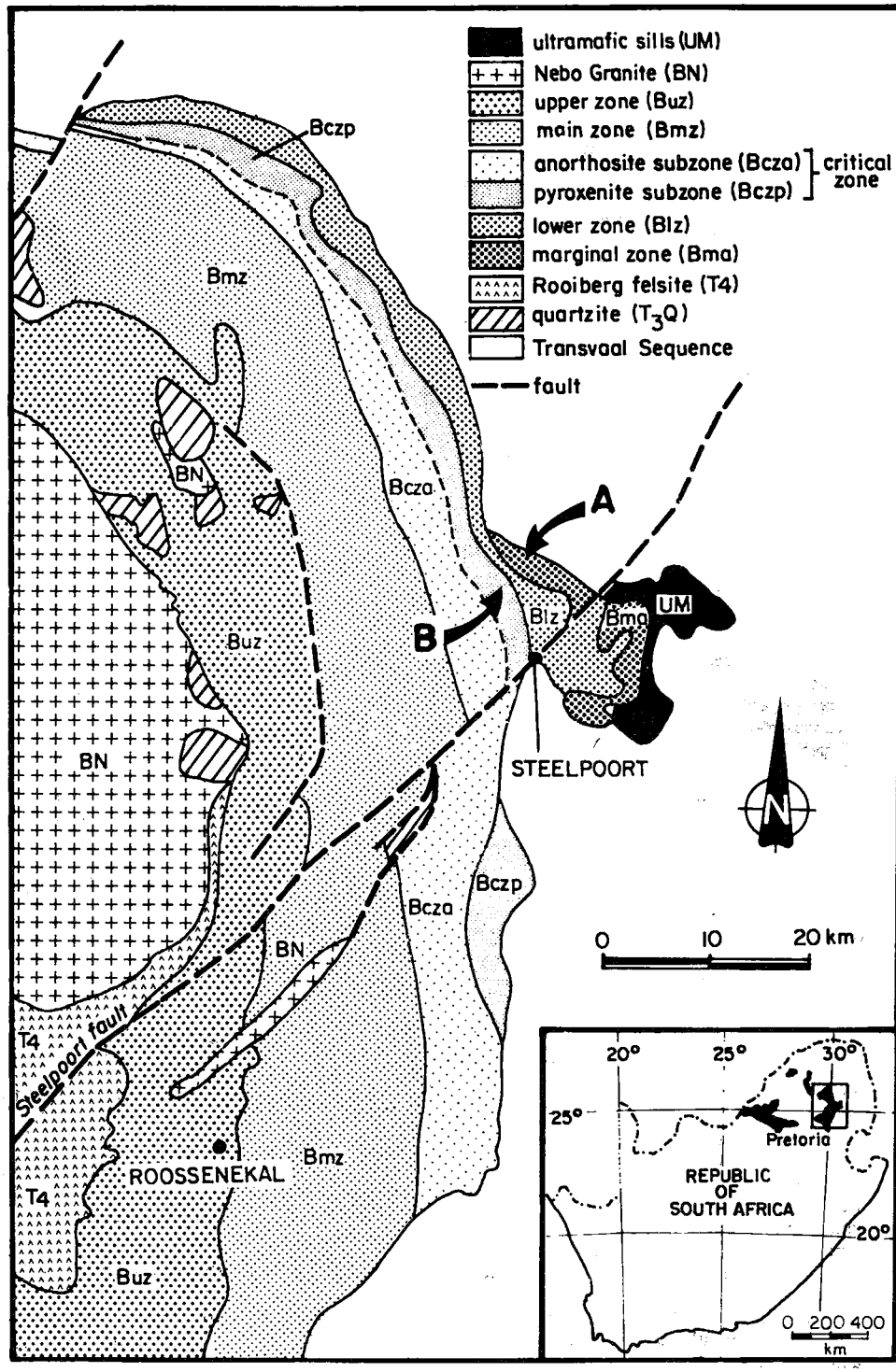


FIG. 1. Geological map of the eastern Bushveld Complex. Arrows A and B refer to the location of the calc-silicate xenoliths in the marginal and critical zones, respectively.

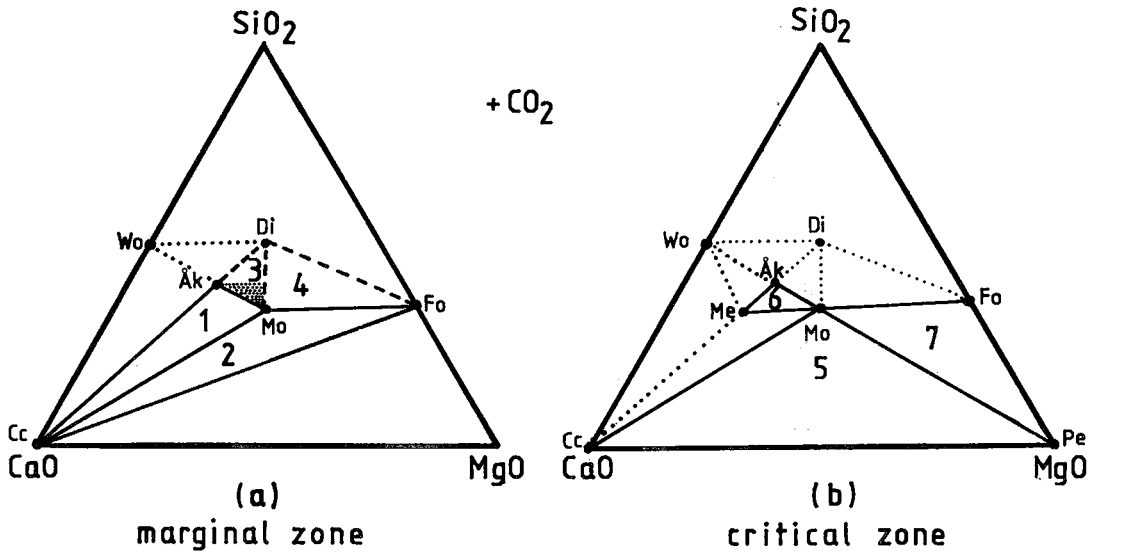


FIG. 2. Compositional triangles showing the important mineral phases and dominant assemblages in the xenoliths located in the marginal (a) and critical (b) zones. Solid lines and dashed lines connect coexisting minerals occurring during prograde and retrograde metamorphism, respectively; minerals connected by dotted lines do not coexist in the xenoliths. Assumed bulk composition of xenoliths in the marginal zone is indicated by the marked area in the center of Figure 2a. Numbers refer to assemblages listed in the text.

From the experimental work of Walter (1963), Willemse & Bensch (1964) concluded that a $T$ greater than 900°C must have prevailed in the xenoliths. Willemse & Bensch (1964) reported kalsilite from a xenolith in the marginal zone and gave a chemical composition of a mineral mixture in which kalsilite participates. Kalsilite is extremely rare and is mostly found as an igneous mineral in volcanic areas. The only occurrence of kalsilite as a metamorphic mineral has been reported from a calc-silicate xenolith from Brome Mountain, Quebec (Philpotts *et al.* 1967), where the kalsilite is associated with melilite, diopside and spinel. In the present paper, we present an average composition derived from 10 microprobe analyses of kalsilite in a xenolith in the marginal zone, and we confirm the metamorphic occurrence of kalsilite.

One of our aims in the present study is to give further insight into the petrogenesis and stability fields of mineral parageneses and mineral reactions pertinent to xenoliths in the marginal zone, as well as merwinite- and periclase-bearing xenoliths in the critical zone (arrow B in Fig. 1). The xenoliths are relatively small (several 1000 $m^3$) and either oval or wedge-shaped. Their exact origin remains ambiguous, but they presumably are remnants of sediments of the Transvaal Sequence, into which the Bushveld magmas were intruded (Willemse & Bensch 1964).

The small size of the xenoliths suggests that they attained thermal equilibrium with the surrounding magma relatively quickly. The time $t$ taken for equilibration may be estimated roughly from the equation $t = x^2/K$, where $x$ is the scale length and $K$ the thermal diffusivity (England & Thompson 1984). For a xenolith of radius 5 m and diffusivity $10^{-6}$ $m^2s^{-1}$, $t$ is *ca.* 0.8 years, which is several orders of magnitude smaller than the likely cooling time for the *ca.* 9-km-thick Bushveld Complex.

## Mineral Parageneses

The xenoliths contain combinations of the following minerals (formulae given for dominant end-members only): åkermanite-rich melilite ($Ca_2MgSi_2O_7$; Åk), monticellite ($CaMgSiO_4$; Mo), diopsidic clinopyroxene ($CaMgSi_2O_6$; Di), forsteritic olivine ($Mg_2SiO_4$; Fo), merwinite [$Ca_3MgSi_2O_8$; Me), periclase (MgO; Pe), brucite [$Mg(OH)_2$], spinel ($MgAl_2O_4$), calcite ($CaCO_3$; Cc), wollastonite ($CaSiO_3$; Wo), kalsilite ($KAlSiO_4$), Ba-rich phlogopite [$K_2Mg_6Si_6Al_2O_{20}(OH)_4$] and apatite [$Ca_5(PO_4)_3(Cl,F)$].

Two different groups of calc-silicates can be distinguished on the bases of field occurrence and mineral assemblage. The first, which occurs in a gabbronorite of the marginal zone, consists of melilite, monticellite, aluminian augite, diopside, forsterite, calcite, and accessory spinel, kalsilite, Ba-rich phlogopite, wollastonite and apatite. The second group occurs in xenoliths in a feldspathic pyroxenite

in the lower critical zone, and consists of monticellite, merwinite, melilite, and periclase mostly altered to brucite. Spinel is the only accessory mineral. The mineralogical and petrological features are, in some respects, similar to those described for the Cascade Slide xenolith in the Adirondacks (Valley & Essene 1980) and monticellite-bearing Adirondack marbles (Tracy 1978). Figure 2 illustrates the compositional relationship of the major mineral phases of the two groups of xenoliths.

Wollastonite is relatively rare in the xenoliths, but there is strong evidence for localized retrograde decomposition of åkermanite to wollastonite and monticellite (Willemse & Bensch 1964). Wollastonite was found only in the outermost part of some xenoliths, where it seems likely that postmagmatic hydrothermal fluids catalyzed this reaction. The occurrence of mostly unaltered åkermanite and forsterite in the xenoliths supports this theory.

Crucial high-grade mineral parageneses in xenoliths in the marginal zone (Fig. 2a) are:

1) calcite – åkermanite – monticellite,
2) calcite – forsterite – monticellite,
3) åkermanite – diopside – monticellite,
4) diopside – forsterite – monticellite.

These are assemblages of minerals that are observed in mutual contact. The mineral assemblage monticellite – wollastonite, resulting from the previously mentioned retrograde reaction of åkermanite, is not shown. The minerals connected by dashed lines in Figure 2a coexist only in retrograde mineral assemblages displaying symplectitic textures (assemblages 3 and 4 in Fig. 2a). The peak metamorphic assemblage giving rise to retrograde assemblages 3 and 4 is åkermanite + forsterite. Although these two minerals are never in contact, they clearly coexisted prior to retrogression. The minerals connected by dotted lines in Figure 2a do not coexist. Assemblages 1 and 2 appear in coarse polygonal textures and indicate peak metamorphic conditions. Assemblages that occur in xenoliths in the critical zone are:

5) calcite – periclase – monticellite,
6) merwinite – åkermanite – monticellite
7) forsterite – periclase – monticellite,

and are represented in Figure 2b.

Tables 1 and 2 present a compilation of mineral assemblages together with textural features and microprobe data pertaining to the important minerals in these assemblages. Figures 3 to 7 show the important minerals, mineral assemblages and the different textural features.

Modal analyses of the layered rocks indicate that the original lithology was a siliceous dolomite with a bulk composition plotting somewhere near the center of the compositional triangles (Figs. 2a, b). This inference is borne out by the crucial mineral parageneses. The shaded triangle in the center of Figure 2a is the only compositional field common to the most abundant minerals and mineral assemblages.

Xenoliths in the critical zone contain less silica than those in the marginal zone. The appearance of periclase in xenoliths in the critical zone is probably due not only to metamorphic conditions but also to a higher Mg content. The latter might have been caused by metasomatism, as the chemical potential of Mg in the magma, which formed a feldspathic pyroxenite, was higher than in the xenoliths which, in turn, had higher chemical potentials of Si and Ca. In the marginal zone, the gabbroic magma and the xenoliths had similar chemical potentials with respect to Si, Mg and Ca, so that the metasomatic effects on the bulk composition are less marked.

## Petrogenetic Grid

To obtain the stability fields of the observed mineral parageneses, it is necessary to compute all possible reaction curves involving subsets of eight relevant $CaO$–$MgO$–$SiO_2$–$CO_2$ minerals and a $CO_2$-bearing fluid, with pressure, temperature and composition of the fluid phase as variables. The total number of $CO_2$-saturated invariant points in the complete multisystem calcite, periclase, forsterite, monticellite, merwinite, åkermanite, diopside and wollastonite is 56. This set may be reduced to 36 by precluding all equilibria in which periclase and wollastonite coexist. (To our knowledge, this assemblage

TABLE 1. MINERAL ASSEMBLAGES FOUND IN XENOLITHS OF THE MARGINAL AND CRITICAL ZONES

| Mineral\Sample | J8 | I3 | J6 | J21 | W1 | W7 | Wa |
|---|---|---|---|---|---|---|---|
| melilite | $X_{1,2}$ | | $X_2$ | | $X_2$ | | |
| monticellite | $X_7$ | $X_{2,8}$ | $O_7$ | | $X_8$ | X | $X_8$ |
| clinopyroxene | $X_1$ | | | X | | | |
| olivine | $X_1$ | $O_6$ | | X | $O_6$ | $X_9$ | $X_6$ |
| spinel | $O_3$ | $O_3$ | $X_{2,3}$ | | $O_3$ | $O_3$ | $X_{3,10}$ |
| phlogopite | $O_{12}$ | | $O_{11}$ | X | | | |
| kalsilite | | | | $O_7$ | | | |
| wollastonite | | | $O_7$ | | | | |
| merwinite | | | | | $X_2$ | | |
| periclase | | | | | | $O_{12}$ | $O_{12}$ |
| brucite | | | | | | X | X |
| calcite | $O_5$ | $X_5$ | $X_5$ | | | $O_5$ | $X_5$ |

X: Essential mineral O: Accessory mineral (<2 vol.%)
Sample J8, I3, J6, J21: marginal zone; W1, W7, Wa: critical zone; 1: symplectic intergrowth; 2: polygonal grains; 3: inclusions in all present phases but calcite; 4: inclusions in melilite; 5: inclusions in melilite and monticellite; 6: exsolutions in monticellite and intergranular; 7: decomposition product of melilite; 8: displays exsolutions of forsterite; 9: relict in brucite; 10: intergranular; 11: as inclusions in melilite; 12: inclusions in brucite.

TABLE 2. REPRESENTATIVE CHEMICAL COMPOSITION OF THE MINERALS

| | Mer. | Per. | Melilite | | | | | | Monticellite | | | | | Clinopyrox. | |
|---|---|---|---|---|---|---|---|---|---|---|---|---|---|---|---|
| | W1 | W7 | J8(1) | J8(2) | J6(2) | J6(2a) | W1(2a) | W1(2b) | J8(7) | I3(2,8) | W1(8) | W7 | Wa(8) | J8(1) | J21 |
| $SiO_2$ | 35.64 | 0.01 | 42.28 | 42.44 | 35.08 | 42.23 | 33.21 | 28.49 | 37.39 | 37.37 | 37.91 | 37.64 | 38.20 | 46.08 | 52.87 |
| $TiO_2$ | 0.03 | 0.00 | 0.02 | 0.01 | 0.00 | 0.00 | 0.00 | 0.00 | 0.01 | 0.04 | 0.02 | 0.03 | 0.03 | 2.09 | 0.54 |
| $Al_2O_3$ | 0.00 | 0.00 | 5.80 | 3.71 | 16.74 | 4.86 | 16.04 | 24.18 | 0.00 | 0.00 | 0.01 | 0.00 | 0.01 | 9.31 | 2.06 |
| $Cr_2O_3$ | 0.01 | 0.03 | 0.00 | 0.00 | 0.00 | 0.00 | 0.02 | 0.00 | 0.03 | 0.01 | 0.02 | 0.01 | 0.00 | 0.00 | 0.05 |
| $Fe_2O_3$ * | 0.00 | 0.00 | 0.00 | 0.00 | 0.00 | 0.00 | 0.00 | 0.00 | 0.00 | 0.00 | 0.00 | 0.00 | 0.00 | 1.40 | 0.00 |
| FeO | 0.30 | 3.54 | 0.69 | 0.83 | 0.61 | 0.85 | 0.68 | 0.79 | 4.01 | 1.37 | 0.60 | 0.61 | 0.51 | 2.21 | 1.49 |
| MnO | 0.01 | 0.12 | 0.03 | 0.00 | 0.04 | 0.03 | 0.01 | 0.01 | 0.29 | 0.10 | 0.31 | 0.31 | 0.18 | 0.05 | 0.03 |
| MgO | 11.60 | 96.23 | 10.90 | 11.84 | 7.11 | 11.70 | 7.91 | 4.68 | 22.20 | 25.31 | 25.48 | 25.70 | 25.91 | 13.44 | 16.88 |
| CaO | 52.19 | 0.00 | 38.94 | 39.85 | 40.06 | 39.99 | 41.59 | 41.66 | 35.82 | 35.84 | 35.71 | 35.73 | 35.13 | 25.48 | 25.83 |
| $Na_2O$ | 0.00 | 0.00 | 1.06 | 1.08 | 0.30 | 0.31 | 0.03 | 0.04 | 0.00 | 0.01 | 0.02 | 0.00 | 0.00 | 0.00 | 0.00 |
| $K_2O$ | 0.00 | 0.00 | 0.23 | 0.32 | 0.03 | 0.04 | 0.04 | 0.03 | 0.00 | 0.00 | 0.00 | 0.00 | 0.00 | 0.00 | 0.00 |
| Total | 99.78 | 99.93 | 99.95 | 100.08 | 99.98 | 100.01 | 99.53 | 99.88 | 99.75 | 100.05 | 100.07 | 100.01 | 99.97 | 100.06 | 99.75 |
| For-mula | 8(0) | 1(0) | 7(0) | | | | | | 4(0) | | | | | 6(0) | |
| Si | 1.97 | 0.00 | 1.91 | 1.93 | 1.59 | 1.91 | 1.53 | 1.31 | 1.00 | 0.98 | 0.99 | 0.99 | 1.00 | 1.69 | 1.93 |
| Ti | 0.00 | 0.00 | 0.03 | 0.00 | 0.00 | 0.00 | 0.00 | 0.00 | 0.00 | 0.00 | 0.00 | 0.00 | 0.00 | 0.06 | 0.01 |
| Al | 0.00 | 0.00 | 0.31 | 0.20 | 0.90 | 0.26 | 0.87 | 1.31 | 0.00 | 0.00 | 0.00 | 0.00 | 0.00 | 0.40 | 0.09 |
| $Cr^{3+}$ | 0.00 | 0.00 | 0.00 | 0.00 | 0.00 | 0.00 | 0.00 | 0.00 | 0.00 | 0.00 | 0.00 | 0.00 | 0.00 | 0.00 | 0.00 |
| $Fe^{3+}$ * | 0.00 | 0.00 | 0.00 | 0.00 | 0.00 | 0.00 | 0.00 | 0.00 | 0.00 | 0.00 | 0.00 | 0.00 | 0.00 | 0.04 | 0.00 |
| $Fe^{2+}$ | 0.01 | 0.02 | 0.03 | 0.03 | 0.02 | 0.03 | 0.03 | 0.03 | 0.09 | 0.03 | 0.01 | 0.01 | 0.01 | 0.07 | 0.05 |
| Mn | 0.00 | 0.00 | 0.00 | 0.00 | 0.00 | 0.00 | 0.00 | 0.00 | 0.01 | 0.00 | 0.01 | 0.01 | 0.00 | 0.00 | 0.00 |
| Mg | 0.95 | 0.98 | 0.74 | 0.80 | 0.48 | 0.79 | 0.54 | 0.32 | 0.88 | 0.99 | 0.99 | 1.00 | 1.01 | 0.74 | 0.92 |
| Ca | 3.09 | 0.00 | 1.89 | 1.94 | 1.95 | 1.94 | 2.06 | 2.05 | 1.02 | 1.00 | 1.00 | 1.00 | 0.98 | 1.00 | 1.01 |
| Na | 0.00 | 0.00 | 0.09 | 0.10 | 0.03 | 0.03 | 0.00 | 0.00 | 0.00 | 0.00 | 0.00 | 0.00 | 0.00 | 0.00 | 0.00 |
| K | 0.00 | 0.00 | 0.01 | 0.02 | 0.00 | 0.00 | 0.00 | 0.00 | 0.00 | 0.00 | 0.00 | 0.00 | 0.00 | 0.00 | 0.00 |
| Total | 6.02 | 1.00 | 5.01 | 5.02 | 4.97 | 4.96 | 5.03 | 5.02 | 3.00 | 3.00 | 3.01 | 3.01 | 3.00 | 4.00 | 4.01 |

| | Olivine | | | | | Spinel | | | | | Kals. | Lar. | Ba-Phl. | | |
|---|---|---|---|---|---|---|---|---|---|---|---|---|---|---|---|
| | J8(1) | I3(6) | J21 | W7(9) | Wa(6) | J6 | J8 | W7 | I3 | Wa | J21 | J8 | J21 | J6(a) | J6(b) |
| $SiO_2$ | 41.87 | 41.83 | 41.35 | 42.07 | 41.93 | 0.04 | 0.05 | 0.04 | 0.00 | 0.03 | 37.84 | 35.73 | 36.74 | 31.21 | 31.67 |
| $TiO_2$ | 0.00 | 0.00 | 0.00 | 0.00 | 0.00 | 0.09 | 0.02 | 0.46 | 0.11 | 0.65 | 0.00 | 0.00 | 0.00 | 3.33 | 3.30 |
| $Al_2O_3$ | 0.01 | 0.02 | 0.02 | 0.01 | 0.00 | 67.25 | 66.13 | 61.26 | 70.01 | 61.79 | 31.13 | 0.07 | 15.86 | 18.91 | 18.50 |
| $Cr_2O_3$ | 0.00 | 0.02 | 0.01 | 0.00 | 0.00 | 0.00 | 0.17 | 0.11 | 0.01 | 0.14 | 0.00 | 0.01 | 0.01 | 0.00 | 0.00 |
| $Fe_2O_3$ * | 0.20 | 1.30 | 0.95 | 0.66 | 0.67 | 3.44 | 4.66 | 10.93 | 1.12 | 9.74 | 0.00 | 0.00 | 1.42 | 2.54 | 2.34 |
| FeO | 3.24 | 0.00 | 4.07 | 0.00 | 0.00 | 3.97 | 3.87 | 0.40 | 1.51 | 0.85 | 0.46 | 0.18 | 0.00 | 0.00 | 0.00 |
| MnO | 0.30 | 0.09 | 0.18 | 0.28 | 0.27 | 0.11 | 0.20 | 0.12 | 0.02 | 0.20 | 0.02 | 0.00 | 0.02 | 0.04 | 0.04 |
| MgO | 53.95 | 55.97 | 53.02 | 56.88 | 56.82 | 25.31 | 25.15 | 27.37 | 27.17 | 27.02 | 0.00 | 0.00 | 25.70 | 23.03 | 23.66 |
| CaO | 0.40 | 0.87 | 0.36 | 0.37 | 0.39 | 0.05 | 0.04 | 0.00 | 0.01 | 0.00 | 0.01 | 63.54 | 0.00 | 0.04 | 0.17 |
| BaO | 0.00 | 0.00 | 0.00 | 0.00 | 0.00 | 0.00 | 0.00 | 0.00 | 0.00 | 0.00 | 0.00 | 0.00 | 7.21 | 12.69 | 14.60 |
| $Na_2O$ | 0.00 | 0.00 | 0.00 | 0.00 | 0.00 | 0.00 | 0.00 | 0.00 | 0.00 | 0.00 | 0.00 | 0.00 | 0.00 | 0.03 | 0.05 |
| $K_2O$ | 0.00 | 0.00 | 0.03 | 0.00 | 0.00 | 0.00 | 0.01 | 0.00 | 0.01 | 0.00 | 30.42 | 0.10 | 8.84 | 6.23 | 5.77 |
| $H_2O$ ** | | | | | | | | | | | | | 4.20 | 1.95 | 0.00 |
| Total | 99.97 | 100.10 | 99.99 | 100.27 | 100.08 | 100.26 | 100.30 | 100.69 | 99.97 | 100.42 | 99.88 | 99.63 | 100.00 | 100.00 | 100.10 |
| For-mula | | | 4(0) | | | | | 4(0) | | | 4(0) | 4(0) | | 22(0) norm. | |
| Si | 1.00 | 0.99 | 0.99 | 0.99 | 0.99 | 0.00 | 0.00 | 0.00 | 0.00 | 0.00 | 1.01 | 1.04 | 5.44 | 4.67 | 4.69 |
| Ti | 0.00 | 0.00 | 0.00 | 0.00 | 0.00 | 0.00 | 0.00 | 0.01 | 0.00 | 0.01 | 0.00 | 0.00 | 0.00 | 0.37 | 0.37 |
| Al | 0.00 | 0.00 | 0.00 | 0.00 | 0.00 | 1.93 | 1.91 | 1.78 | 1.98 | 1.80 | 0.97 | 0.02 | 2.78 | 3.34 | 3.31 |
| $Cr^{3+}$ | 0.00 | 0.00 | 0.00 | 0.00 | 0.00 | 0.00 | 0.00 | 0.00 | 0.00 | 0.00 | 0.00 | 0.00 | 0.00 | 0.00 | 0.00 |
| $Fe^{3+}$ * | 0.00 | 0.02 | 0.02 | 0.01 | 0.01 | 0.07 | 0.09 | 0.20 | 0.02 | 0.18 | 0.00 | 0.00 | 0.02 | 0.29 | 0.26 |
| $Fe^{2+}$ | 0.06 | 0.00 | 0.08 | 0.00 | 0.00 | 0.08 | 0.08 | 0.01 | 0.03 | 0.02 | 0.01 | 0.00 | 0.00 | 0.00 | 0.00 |
| Mn | 0.01 | 0.00 | 0.00 | 0.00 | 0.00 | 0.00 | 0.00 | 0.00 | 0.00 | 0.00 | 0.00 | 0.00 | 0.00 | 0.00 | 0.00 |
| Mg | 1.92 | 1.97 | 1.90 | 1.99 | 1.99 | 0.92 | 0.92 | 1.00 | 0.97 | 0.99 | 0.00 | 0.00 | 5.67 | 5.13 | 5.22 |
| Ca | 0.01 | 0.02 | 0.01 | 0.01 | 0.01 | 0.00 | 0.00 | 0.00 | 0.00 | 0.00 | 0.00 | 1.95 | 0.00 | 0.01 | 0.03 |
| Ba | 0.00 | 0.00 | 0.00 | 0.00 | 0.00 | 0.00 | 0.00 | 0.00 | 0.00 | 0.00 | 0.00 | 0.00 | 0.42 | 0.74 | 0.85 |
| Na | 0.00 | 0.00 | 0.00 | 0.00 | 0.00 | 0.00 | 0.00 | 0.00 | 0.00 | 0.00 | 0.00 | 0.00 | 0.00 | 0.01 | 0.01 |
| K | 0.00 | 0.00 | 0.00 | 0.00 | 0.00 | 0.00 | 0.00 | 0.00 | 0.00 | 0.00 | 1.03 | 0.00 | 1.67 | 1.19 | 1.09 |
| Total (OH,F) ($O_2$) | 3.00 | 3.00 | 3.00 | 3.00 | 3.00 | 3.00 | 3.00 | 3.00 | 3.00 | 3.00 | 3.02 | 3.01 | 16.00 (0.00) (4.15) | 15.75 (1.94) (2.06) | 15.83 (0.00) (4.00) |

Chemical data obtained by electron microprobe (see text). Minerals from xenoliths in the marginal zone are designated I or J, whereas those in the critical zone are designated W. * Recalculated (Finger 1972). ** Estimated to obtain 100 wt.%.

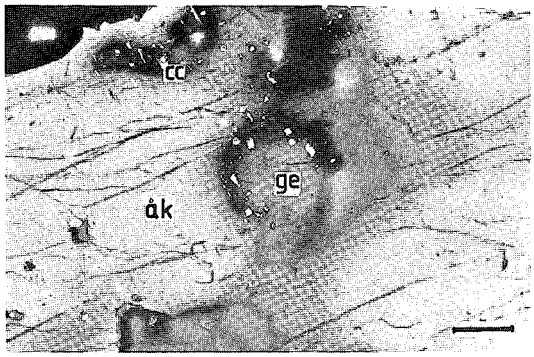


FIG. 3. Melilite with changing composition from core (gehlenite) toward grain boundary (åkermanite). The small (white) inclusions consist of calcite. Bar represents 0.35 mm; crossed polars.

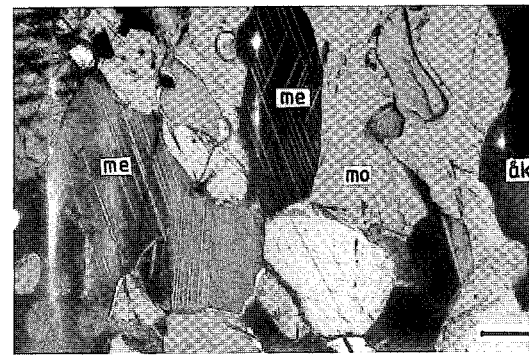


FIG. 6. Merwinite with typical twin lamellae in two directions together with monticellite and åkermanite. Bar represents 0.35 mm; crossed polars.

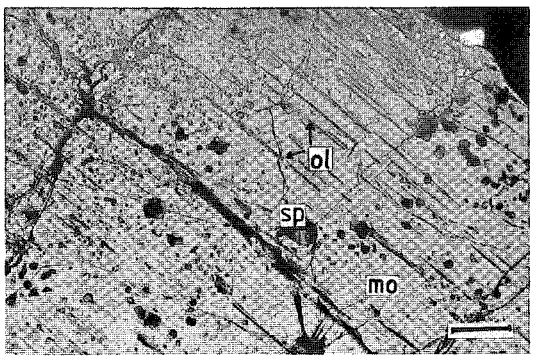


FIG. 4. Forsterite exsolution lamellae in monticellite. Isotropic (black) inclusions are spinel. Bar represents 0.35 mm; crossed polars.

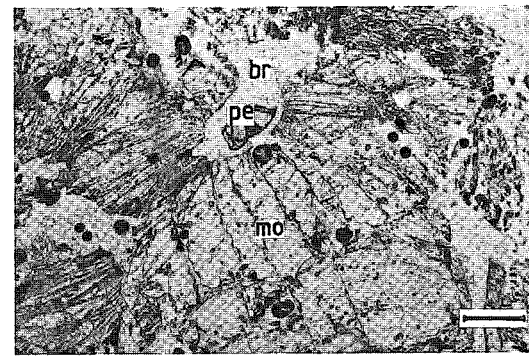


FIG. 7. Periclase partly altered to brucite in monticellite. Bar represents 0.35 mm; uncrossed polars.

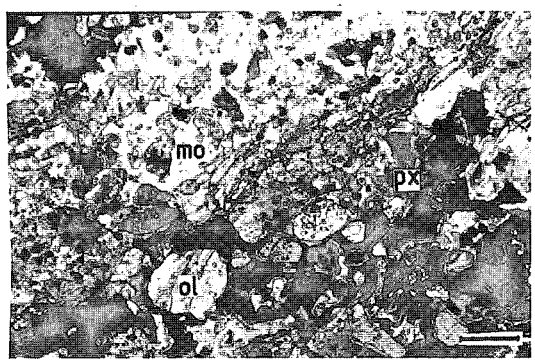


FIG. 5. Symplectitic intergrowth of monticellite–diopside–forsterite. Small inclusions within olivine are spinel. Bar represents 0.35 mm; crossed polars.

has never been recorded from experiments or natural rocks.) We have constructed a petrogenetic grid for these 36 remaining invariant points (Fig. 8). The 32 univariant reaction curves linking these points are listed in Table 3. Of these, reactions 1–20 involve phases in Figure 2a, whereas reactions 12–32 involve those in Figure 2b. Although the petrogenetic grid is distorted for space reasons, we emphasize that the relative positions of the invariant points are still preserved.

The invariant points (Table 4) have been subdivided into stable and metastable with respect to the stability or metastability of the intersecting univariant reaction-curves. This has been done by geometrical analysis and application of the rules of Schreinemakers (*e.g.*, Zen 1966, Roseboom & Zen 1982, Guo 1984). Invariant points that are metasta-

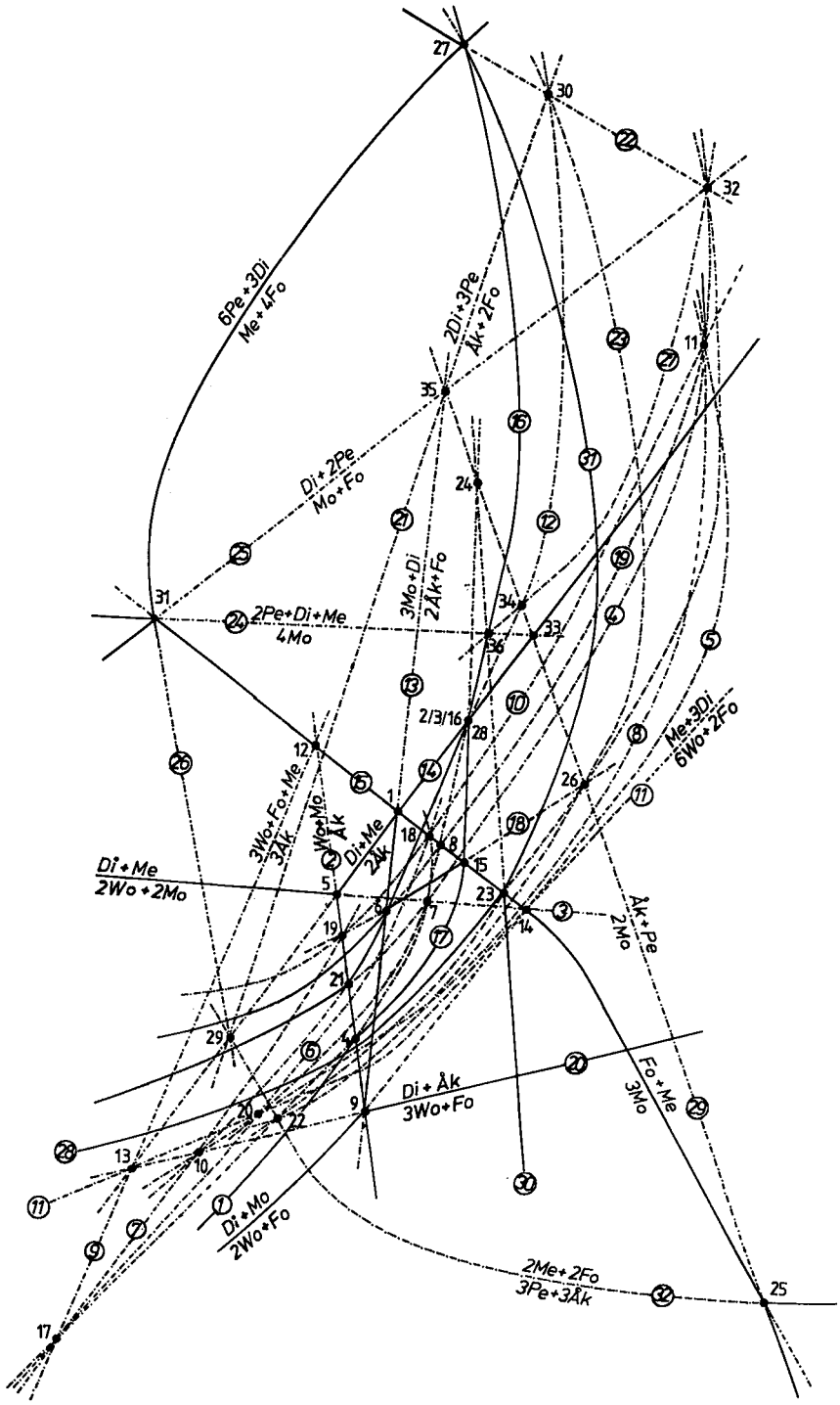


FIG. 8. Petrogenetic grid comprising stable (solid lines) and metastable reactions (dashed lines), and invariant points, given in Tables 3 and 4.

TABLE 3. HIGH-TEMPERATURE REACTIONS IN THE CALCITE-WOLLASTONITE-MONTICELLITE-MERWINITE-ÅKERMANITE-DIOPSIDE-FORSTERITE-PERICLASE MULTISYSTEM IN THE SYSTEM $CaO$-$MgO$-$SiO_2$-$CO_2$

| | |
|---|---|
| 1)x Cc + Wo + Mo = Me + $CO_2$ | 17)x Cc + Åk = Me + $CO_2$ |
| 2)x Wo + Mo = Åk | 18)x Cc + Fo + Åk = 3Mo +$CO_2$ |
| 3)x 2Wo + 2Mo = Di + Me | 19)x Cc + Di + Fo = 3Mo + $2CO_2$ |
| 4)x Cc + Di = Wo + Mo + $CO_2$ | 20) 3Wo + Fo = Di + Åk |
| 5) Mo + Di = 2Wo + Fo | 21) 3Fo + Åk = 2Di + 3Pe |
| 6) 3Cc + 3Wo + Fo = 2Me + $3CO_2$ | 22) Cc + 2Fo = Di + 3Pe + $CO_2$ |
| 7) Cc + 3Wo + Fo = 2Åk + $CO_2$ | 23) 2Cc + 2Fo = Åk + 3Pe + $2CO_2$ |
| 8) Cc + 2Di = 3Wo + Fo+ $CO_2$ | 24)x 2Pe + Di + Me = 4Mo |
| 9) 3Wo + Fo + Me = 3Åk | 25)x Mo + Fo = Di + 2Pe |
| 10) Cc + Wo + Fo = 2Mo + $CO_2$ | 26)x Me + 4Fo = 6Pe + 3Di |
| 11) Me + 3Di = 6Wo + 2Fo | 27) Cc + Pe + Di = 2Mo + $CO_2$ |
| 12)x Cc + Di = Åk+ $CO_2$ | 28)x Cc + Fo = Mo + Pe + $CO_2$ |
| 13)x 3Mo + Di = 2Åk + Fo | 29)x Åk + Pe = 2Mo |
| 14)x Di + Me = 2Åk | 30)x Cc + 2Mo = Me + Pe + $CO_2$ |
| 15)x Me + Fo = 3Mo | 31) 3Cc + 2Fo = Me + 3Pe + $3CO_2$ |
| 16) 2Cc + Di = Me + $2CO_2$ | 32)x 2Me + 2Fo = 3Pe + 3Åk |

"x" indicates stable reaction curves (see text)

TABLE 4. THIRTY-SIX INVARIANT POINTS IN THE SYSTEM $CaO$-$MgO$-$SiO_2$-$CO_2$

| | | | |
|---|---|---|---|
| 1) [Cc,Wo,Pe] s | 2) [Fo,Wo,Pe] s | 3) [Fo,Mo,Pe] s | 4) [Fo,Di,Pe] s |
| 5) [Cc,Fo,Pe] s | 6) [Wo,Me,Pe] s | 7) [Fo,Åk,Pe] m | 8) [Wo,Åk,Pe] m |
| 9) [Cc,Me,Pe] m | 10) [Mo,Me,Pe] m | 11) [Me,Åk,Pe] m | 12) [Cc,Di,Pe] m |
| 13) [Cc,Mo,Pe] m | 14) [Cc,Åk,Pe] m | 15) [Wo,Di,Pe] s | 16) [Wo,Mo,Pe] s |
| 17) [Di,Mo,Pe] m | 18) [Di,Åk,Pe] m | 19) [Me,Di,Pe] m | 20) [Mo,Åk,Pe] m |
| 21) [Fo,Me,Pe] s | 22) [Di,Mo,Wo] m | 23) [Di,Åk,Wo] s | 24) [Di,Fo,Wo] m |
| 25) [Cc,Di,Wo] m | 26) [Di,Me,Wo] m | 27) [Åk,Mo,Wo] s | 28) [Mo,Fo,Wo] s |
| 29) [Cc,Mo,Wo] m | 30) [Mo,Me,Wo] m | 31) [Cc,Åk,Wo] s | 32) [Åk,Me,Wo] m |
| 33) [Cc,Fo,Wo] m | 34) [Fo,Me,Wo] m | 35) [Cc,Me,Wo] m | 36) [Åk,Fo,Wo] m |

Phases in brackets do not participate in the reactions that intersect at the respective invariant points; s=stable, m=metastable.

ble with respect to unrealistic P–T conditions ("negative" pressures or temperatures, or very high pressures at very low temperatures) also shall be referred to as metastable. These include, for example, invariant points 9 and 25, which appear to be "geometrically" stable, although they would occur at "negative" pressures. The invariant points and reactions that are stable over a realistic P–T range, reflecting mainly contact-metamorphic conditions, are shown in Figure 9. The 14 stable reactions are marked with an "x" in Table 3.

The actual P–T coordinates of the reaction curves were calculated using a thermodynamic data-set given in Table 5. The enthalpy of formation of merwinite has been adapted to Yoder's (1968) experimental results ($\Delta H^\circ_{298} = -1{,}085{,}060$ cal) and is slightly different from the value ($\Delta H^\circ_{298} = -1{,}084{,}506$ cal) ascertained by Brousse *et al.* (1984). Although more recent data on heat capacities and third-law entropies of åkermanite (Hemingway *et al.* 1986) and monticellite (Sharp *et al.* 1986) are available, the thermodynamic data used in this paper fit the experimental data equally well.

## Composition of the Fluid Phase

The occurrence of decarbonation reactions can be facilitated by lowering the values of the $CO_2$ pressures, as discussed by Tracy (1978) and Valley & Essene (1980) for decarbonation reactions producing melilite- and monticellite-bearing mineral assemblages in the Adirondacks. The lowering of the $CO_2$ pressure can be achieved by diluting $CO_2$ with $H_2O$, resulting in lower temperatures of reaction for decarbonation reactions. Some aspects concerning the mixing behavior of $CO_2$ and $H_2O$ under the extreme conditions that led to the formation of monticellite-, åkermanite-, merwinite-, and periclase-bearing assemblages are discussed in the Appendix.

Mineral reactions and invariant points at $X(CO_2) = 1$ are shown in Figure 9. During the formation of the specific high-temperature mineral assemblages found in the Bushveld xenoliths, a fluid phase with $X(CO_2)$ near unity can be deduced from the following considerations:

1) The decomposition and dehydration of hydroxyl-bearing minerals usually occur at much lower temperatures than those reached within the xenoliths. In general, low-temperature fluids are dominated by $H_2O$, but the content of $CO_2$ increases with grade if carbonate rocks are present (Fyfe *et al.* 1978). With the exception of minor amounts of partly dehydroxylated Ba-rich phlogopite (see below), no water-bearing minerals are found.

2) Influx of water into the xenolith during decarbonation is improbable because the decarbonation reactions ensured that partial pressure of the fluid phase within the xenolith was equal to total pressure, and the partial pressure of the fluid phase within the surrounding magma was much lower.

3) Water is much more soluble in magma than $CO_2$ (*e.g.*, Burnham 1979). Because the xenoliths were completely surrounded by magma during metamorphism, any $H_2O$ present in the fluid will have tended to diffuse out of the xenoliths into the magma, leaving behind a fluid phase enriched in $CO_2$.

4) Relatively fast heating and concomitant degassing during decarbonation not only result in a loss of volume of *ca.* 40%, but also prohibit magmatic fluids from invading the xenoliths.

5) Fluid inclusions in high-grade rocks, in general, contain high concentrations of $CO_2$ or are almost pure $CO_2$ (Roedder 1984). Very small fluid inclusions, in the form of small specks, as described by Roedder (1984), were found in monticellite and åkermanite and also indicate a very high $X(CO_2)$.

## Evaluation of P and T

### *Marginal zone*

Figure 9 illustrates the reactions that occurred within xenoliths in the marginal and critical zones during prograde and subsequent retrograde

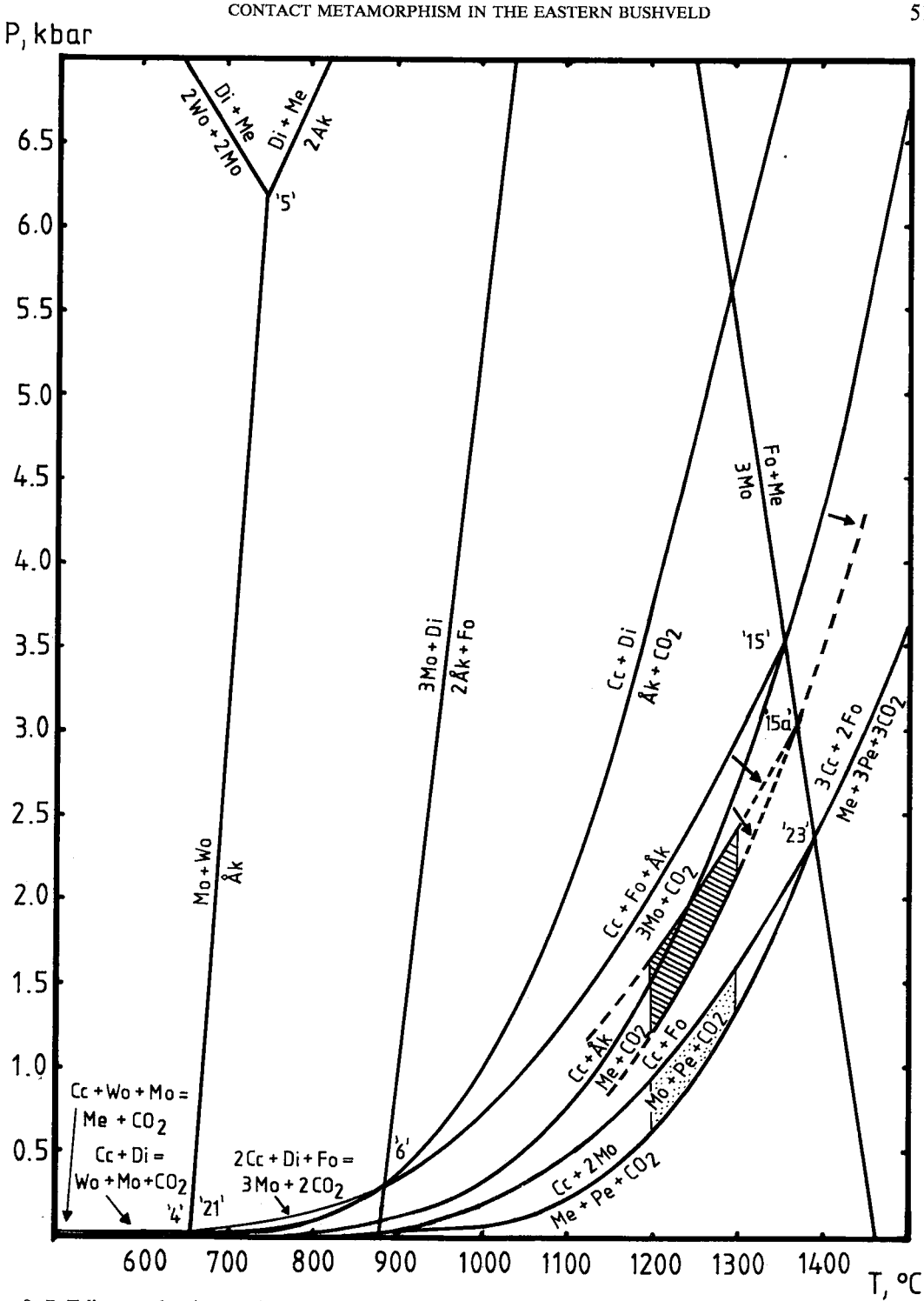


FIG. 9. *P–T* diagram showing possible mineral reactions that can occur during high-temperature metamorphism of siliceous dolomites. Invariant point 15a results from invariant point 15 by using an activity of åkermanite $a_{(Åk)}$ of 0.75. The dashed lines A and B refer to the reactions Cc + Fo + $Åk_{75}$ = 3Mo + $CO_2$ and Cc + $Åk_{75}$ = Me + $CO_2$, respectively. The hatched and the dotted areas indicate the *P–T* conditions under which the marginal and the critical zone magma intruded.

TABLE 5. THERMODYNAMIC PROPERTIES OF THE END MEMBERS

| Mineral | H | S | V | a | b x10$^{-3}$ | c x10$^{5}$ | AT x10$^{-5}$ | BP x10$^{-6}$ |
|---|---|---|---|---|---|---|---|---|
| åkermanite | -923777.0$_a$ | 50.030 | 2.2180 | 60.090 | 11.400 | -11.400 | 7.0985$_b$ | 2.6291$_c$ |
| calcite | -288772.0$^a$ | 22.150 | 0.8830 | 24.980 | 5.240 | -6.200 | 2.1511$_d$ | 1.2667$_d$ |
| diopside | -765598.0 | 34.200 | 1.5800 | 52.800 | 7.840 | -15.740 | 5.2581$_d$ | 1.3145$_d$ |
| dolomite | -556851.0 | 37.090 | 1.5384 | 41.557 | 23.952 | -9.884 | 3.7285$_d$ | 1.5774$_d$ |
| forsterite | -520000.0 | 22.750 | 1.0470 | 35.810 | 6.540 | -8.520 | 3.8241$_d$ | 0.7648$_d$ |
| gehlenite | -951665.0 | 48.100 | 2.1568 | 63.740 | 8.000 | -15.120 | 5.4971$_d$ | 1.9120$_d$ |
| kalsilite | -509408.0 | 31.850 | 1.4314 | 29.430 | 17.360 | -5.320 | 3.5000$_e$ | 2.9200$_c$ |
| leucite | -726255.0$_f$ | 47.850$_f$ | 2.1126$_f$ | 35.470$_f$ | 32.087$_f$ | -5.173$_f$ | 6.0700$_e$ | 4.2100$_c$ |
| monticellite | -537530.0$_a$ | 26.400 | 1.2280 | 36.820 | 5.340 | -8.000 | 4.6606$_b$ | 1.1233$_c$ |
| merwinite | -1085060.0$_a$ | 60.500 | 2.4950 | 72.970 | 11.960 | -14.444 | 9.7275$_b$ | 2.4857$_c$ |
| muscovite | -1427408.0$^g$ | 68.800 | 3.3631 | 97.560 | 26.380 | -25.440 | 10.7600$_d$ | 3.8200$_d$ |
| periclase | -143800.0 | 6.440 | 0.2690 | 10.180 | 1.740 | -1.480 | 1.0994$_d$ | 0.1673$_d$ |
| phlogopite | -1488067.0 | 76.100 | 3.5770 | 100.610 | 28.780 | -21.500 | 11.4700$_d$ | 5.9800$_d$ |
| spinel | -546847.0 | 19.270 | 0.9491 | 36.773 | 6.415 | -9.709 | 2.4618$_d$ | 0.3824$_d$ |
| wollastonite | -389810.0 | 19.600 | 0.9540 | 26.640 | 3.600 | -6.520 | 2.3184$_d$ | 1.1950$_d$ |
| $CO_2$ | -94054.0 | 51.072 | 0.0000 | 10.570 | 2.100 | -2.060 | 0.0000 | 0.0000 |
| $H_2O$ | -57796.0 | 45.104 | 0.0000 | 7.300 | 2.450 | 0.000 | 0.0000 | 0.0000 |

Sources: a) Brousse et al. (1984); b) Skinner (1966); c) estimated by method of Wang (1978) explained in Powell & Holland (1985); d) Holland & Powell (1985); e) estimated as explained in Powell & Holland (1985); f) Robie et al. (1978); g) adapted to experiments of Yoder (1968); all other data from Helgeson et al. (1978).

H: enthalpy of formation from elements at 1 bar and 298 K (cal mole$^{-1}$)
S: third law entropy at 1 bar and 298 K (cal mole$^{-1}$ K$^{-1}$)
V: molar volume at 1 bar and 298 K (cal bar$^{-1}$)
a,b,c: Maier-Kelley coefficients; a (cal mole$^{-1}$ K$^{-1}$)
b (cal mole$^{-1}$ K$^{-2}$)
c (cal mole$^{-1}$ K)
AT: coefficientof thermal expansion multiplied by the molar volume (cal bar$^{-1}$ K$^{-1}$)
PT: coefficient of isothermal compressibility multiplied by the molar volume (cal bar$^{-2}$)

metamorphism. The starting minerals calcite, diopside and forsterite formed at earlier stages of metamorphism (Bowen 1940). On moving from lower to higher temperatures (maintaining $P > 0.4$ kbar), the first reaction-curve crossed is:

3 monticellite + diopside = 2 åkermanite + forsterite.

Because there are no monticellite-forming reactions at low temperatures and high $X(CO_2)$, this reaction usually does not take place. The first reaction that occurs is:

calcite + diopside = åkermanite + $CO_2$.

In some places, depending on the bulk composition, åkermanite and calcite are the only phases present. Diopside is consumed during the åkermanite-producing decarbonation reaction. Åkermanite encloses calcite, proving that this reaction line has been crossed (Fig. 3). The melilite grains are zoned, with the Al contents decreasing toward the rim. Analyses of melilite in samples J6(2) and J6(2a) in Table 2 give an average core and rim conposition, respectively. The compositional changes toward the grain boundaries indicate an increase in temperature for the melilite-producing reaction. By taking the solid solutions of the minerals into consideration, we obtain the following equilibrium constant:

$$K = a_{(\text{Åk})}/a_{(\text{Cc})}a_{(\text{Di})} = 1.01$$

The activities for the minerals were obtained by assuming ideal mixing, which is a simplification for monticellite and clinopyroxene, but relatively realistic for melilite (Charlu *et al.* 1981) and olivine solid-solutions at high temperatures (Saxena 1973):

$$a_{(\text{Åk})} = (X_{\text{Ca}})^2(X_{\text{Mg}})$$
$$a_{(\text{Mo})} = (X_{\text{Ca}})(X_{\text{Mg}})$$
$$a_{(\text{Di})} = (X_{Ca})(X_{\text{Mg}})$$
$$a_{(\text{Fo})} = (X_{Mg})^2$$

The mole fractions have been calculated from Table 2 [åkermanite J8(2): $a_{(\text{Åk})} = 0.75$; clinopyroxene (aluminian augite) J8(1): $a_{(\text{Di})} = 0.74$; $a_{(\text{Cc})}$ equals unity]. Even though $a_{(\text{Di})}$ and $a_{(\text{Åk})}$ deviate considerably from unity, which is mainly due to their Al contents, the equilibrium constant is close to unity, as the activities of the solid solutions cancel each other in the reaction. As $K$ approximately equals 1, the calculated reaction-curves from end-member compositions of the minerals involved can be used.

The activity for åkermanite has been calculated from the rim composition because the outermost parts of the åkermanite grains have been formed at the highest grade of metamorphism.

The next stable reaction-line to be crossed is:

calcite + forsterite + åkermanite = 3 monticellite + $CO_2$.

The mineral parageneses calcite – åkermanite – monticellite and calcite – forsterite – monticellite derive from this reaction. The monticellite produced in this reaction shows exsolution lamellae of forsterite (Fig. 4). Such Fo exsolution lamellae, also described in the Cascade Slide xenolith (Adirondack Mountains) by

Tracy (1978) and Valley & Essene (1980), and in metasedimentary inclusions in the Platreef of the northern limb of the Bushveld Complex (Mostert 1982), are rare in terrestrial rocks, and appear more commonly in chondritic meteorites. Furthermore, this monticellite has an optically positive sign. This property is most unusual and is probably due to the high temperature of formation and subsequent distortion of the crystal structure by solid solution toward the forsterite component. Indices of refraction for this high-temperature monticellite ($\alpha \sim 1.640$, $\beta \sim 1.644$, $\gamma \sim 1.649$), which hosts the forsterite lamellae, indicate a temperature of formation of at least 1200°C (Adams & Bishop 1985). Microprobe analyses show that forsterite and monticellite are very close to end-member compositions [Wa(6), Wa(8), I3(2,8), and I3(6) in Table 2]. Calcite, which is involved in this reaction, has also an end-member composition. The equilibrium constant for the solid phases is:

$$K = a_{(Mo)}{}^3/a_{(\mathring{A}k)}a_{(Fo)}a_{(Cc)} \sim 1.33.$$

The deviation from $K = 1$ is due to Al present in åkermanite, which has a maximum activity of $a_{(\mathring{A}k)} = 0.75$ [J8(2) in Table 4]. Owing to the Al content in åkermanite, all åkermanite-involving reactions, which intersect in invariant point 15 (Fig. 9), become shifted toward higher temperatures (dashed reaction-curves in Fig. 9) and intersect in invariant point 15a. The gehlenite (*i.e.*, aluminous) component in åkermanite reacts to form spinel, which could occur in reactions such as

calcite + 2 forsterite + gehlenite = 3 monticellite + spinel + $CO_2$, or

gehlenite + periclase + forsterite = monticellite + 2 spinel,

where the former occurs during prograde metamorphism, and the latter, during retrograde metamorphism. Alternatively, some of the spinel could have formed at a much lower grade from aluminous precursor-minerals such as Mg-chlorite. No further reaction-line has been crossed during prograde metamorphism in these xenoliths in the marginal zone. During retrograde metamorphism, no decarbonation reaction was reversed, as insufficient $CO_2$ was available. Besides the locally limited reaction

åkermanite = monticellite + wollastonite,

the only retrograde reaction within the Al-free system that can be seen abundantly is the solid–solid reaction

2 åkermanite + forsterite = 3 monticellite + diopside,

which also is shown in Figure 9. This reaction forms a second generation of monticellite (Fig. 5) that displays no forsterite exsolution lamellae and has the usual optical positive sign. Whereas the prograde decarbonation reactions gave rise to polygonal textures, the retrograde solid–solid reaction resulted in a symplectitic intergrowth of åkermanite – diopside – monticellite or diopside – forsterite – monticellite (mineral assemblages 3 and 4 in Fig. 2a), depending on the original bulk-composition (Fig. 5). The resulting "low-temperature" monticellite has the usual negative optical sign. The activity of this monticellite also is lower and does not exceed $a_{(Mo)} = 0.90$. The calculated activities of the minerals within this symplectitic intergrowth are: $a_{(Mo)} = 0.90$; $a_{(\mathring{A}k)} = 0.75$; $a_{(Di)} = 0.74$; $a_{(Fo)} = 0.92$. These activities refer to the microprobe analyses of monticellite [J8(7)], melilite [J8(2)], aluminian augite clinopyroxene [J8(1)] and forsterite [J8(1)]. The equilibrium constant is:

$$K = a_{(Mo)}{}^3a_{(Di)}/a_{(\mathring{A}k)}{}^2a_{(Fo)} = 1.04$$

Although the bulk composition was favorable, the reaction curve

calcite + åkermanite = merwinite + $CO_2$

was not crossed, and no merwinite formed within the in the marginal zone.

As the åkermanite grains in xenoliths in the marginal zone contain between 16.74 wt.% (center) and 3.71 wt.% $Al_2O_3$ (rim), the reactions

calcite + åkermanite + forsterite = 3 monticellite + $CO_2$, and calcite + åkermanite = merwinite + $CO_2$

shift toward higher $T$ and lower $P$ (Fig. 9) to intersect in invariant point 15a. The peak metamorphic conditions calculated from reactions involving åkermanite with an activity $a_{(\mathring{A}k)}$ of 0.75 [*e.g.*, J8(2) in Table 2] is given in the form of a hatched field in Figure 9 that outlines a part of the stability field of the observed mineral parageneses calcite – åkermanite – monticellite and calcite – forsterite – monticellite (mineral assemblages 1 and 2 in Fig. 2a). At magmatic $T$, estimated from 1200 to 1300°C (Irvine & Sharpe 1982), the inferred overload pressure was between 1.1 and 2.4 kbars during the emplacement of the marginal zone magma.

At a $T$ above 1380°C and a $P$ above 3.1 kbars, *i.e.*, on the high $P$–$T$ side of the invariant point 15 and 15a in Figure 9, only the reaction calcite + åkermanite = merwinite + $CO_2$ remains stable, whereas the monticellite-producing decarbonation reaction becomes metastable. The presence of abundant åkermanite and calcite, which did not react to

form merwinite, together with the presence of high-temperature monticellite, lead to the conclusion that the magma $T$ was less than 1390°C, and $P$ did not exceed 3.1 kbars.

*Critical zone*

The critical zone xenoliths are characterized by the presence of merwinite and periclase. By crossing the merwinite-producing reaction

calcite + åkermanite = merwinite + $CO_2$

in Figure 9 and previously mentioned reactions, we obtain the mineral parageneses merwinite – åkermanite – monticellite (Fig. 6 and mineral assemblage 6 in Fig. 2b). The coexistence of periclase and monticellite (Fig. 7), together with the observed mineral assemblages calcite – monticellite – periclase and forsterite – monticellite – periclase (mineral assemblages 5 and 7 in Fig. 2b), are due to the reaction

calcite + forsterite = monticellite + periclase + $CO_2$.

The reaction curve

calcite + 2 monticellite = merwinite + periclase + $CO_2$

has not been crossed, as calcite and monticellite, but not merwinite and periclase, form part of stable parageneses. The equilibrium constant is unity because the phases participating in the monticellite- and periclase-producing reaction have end-member compositions (Table 2). The dotted field in Figure 9 indicates the $P$–$T$ conditions reached during the highest degrees of contact metamorphism in xenoliths in the critical zone.

Using again the Irvine & Sharpe (1982) estimation of magma $T$ between 1200 and 1300°C, the inferred $P$ is between 0.6 and 1.6 kbars. At $T$ greater than 1390°C and $P$ greater than 2.3 kbar, the monticellite- and periclase-forming reaction becomes metastable, and the monticellite–periclase assemblage would not form (Fig. 9). Again, even without having the given constraints on magma $T$, it is possible to conclude that the temperature of the critical zone magma was less than 1400°C, and $P$ did not exceed 2.4 kbars.

## Occurrence of Dehydroxylated Kinoshitalite

The occurrence of a dehydroxylated, Ba-rich phlogopite that formed only under extreme metamorphic conditions bears further evidence of the extreme conditions prevailing in the xenoliths during peak metamorphism. Phlogopite is common in metamorphosed, impure magnesian limestones and dolomites. The chemical composition of the phlogopite that generally occurs in the xenoliths is unusual. The grains are found as inclusions in polygonal åkermanite and monticellite, and in symplectitic intergrowth beside åkermanite, diopside, monticellite and forsterite. One occurrence displays the mineral assemblage Ba-rich phlogopite – kalsilite – forsterite – diopside – wollastonite. Microprobe data for the Ba-rich phlogopite are given in Table 2 (Ba-Phl). The occurrences in åkermanite and monticellite have up to 15 wt.% BaO and can be referred to as kinoshitalite (Ba:K > 1:2; Yoshii & Maeda 1975). In contrast to kinoshitalite from the Noda-Tamagawa mine, Japan (Yoshii & Maeda 1975), most of the Ba-rich phlogopite grains found in the xenoliths are zoned and have outer parts that are, according to the microprobe data, totally devolatilized. The Ba-content increases toward the rim of the mineral, concomitant with an increase of the OH (F,Cl), Al, and K contents toward the center. To date, no dehydroxylated or devolatilized Ba-phlogopite has been recorded in the literature. Trioctahedral micas generally have a very high thermal stability, and the $OH^-$ groups are strongly bound (Olesch 1975). Yoder & Eugster (1955) showed that phlogopite decomposes at high temperatures (Fig. 10) to form orthorhombic kalsilite, leucite, forsterite and $H_2O$ (vapor). In a very localized occurrence at the outermost part of a xenolith, phlogopite with less than 9 wt.% BaO, kalsilite, forsterite, clinopyroxene and wollastonite form a mineral assemblage. Figure 10 shows three reactions that are pertinent to this mineral assemblage. The two prograde reactions describe the formation and the decomposition (Yoder & Eugster 1955) of phlogopite. The lower-temperature reaction, from which the formation of phlogopite in impure magnesian limestones was assumed (*e.g.*, Deer *et al.* 1975), was calculated by means of the thermodynamic data given in Table 5. The presence of clinopyroxene instead of leucite could be expressed by the reaction

2 wollastonite + leucite + forsterite = 2 diopside + kalsilite.

The calculated position of this retrograde reaction also is shown in Figure 10.

The occurrence of isolated Ba-rich phlogopite inclusions in åkermanite and monticellite indicates an increase of the stability field to higher temperatures due to the Ba content. In contrast to this, common phlogopite decomposes at lower temperatures than are necessary for dehydroxylation.

## Summary and Conclusions

The following points define $P$–$T$ conditions reached within the calc-silicate xenoliths:

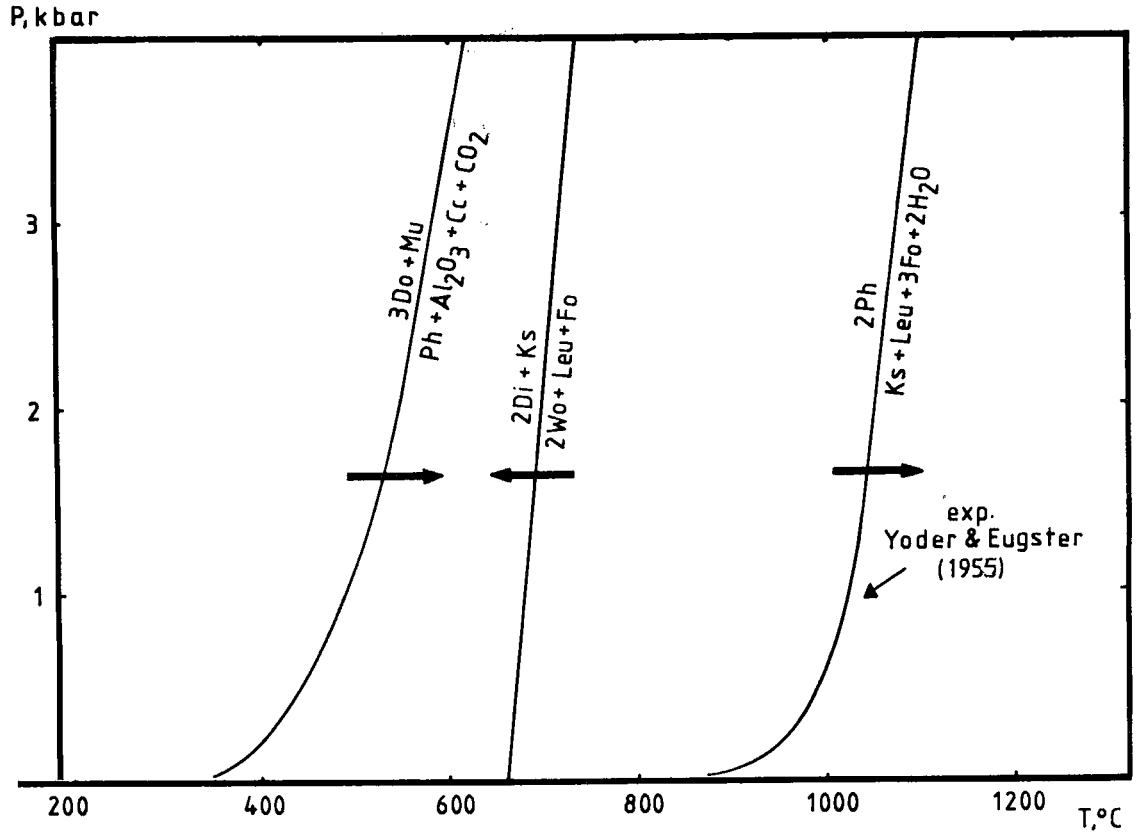


FIG. 10. *P–T* diagram for reactions that account for the prograde formation of phlogopite, kalsilite and leucite, and the retrograde formation of kalsilite that accounts for the missing leucite.

1. The occurrence of exsolved forsterite in a new high-temperature modification of monticellite with a positive optic sign: $T > 1200°C$.
2. The presence of dehydroxylated Ba-rich phlogopite: $T > 1050°C$ (for $> 1$ kbar).
3. The polygonal-textured mineral paragenesis calcite – åkermanite – monticellite in xenoliths in the marginal zone: $T < 1390°C$, $P < 3.1$ kbars.
4. The polygonal-textured mineral paragenesis forsterite – periclase – monticellite in xenoliths in the critical zone: $T < 1390°C$, $P < 2.3$ kbars.

Experimental work (Irvine & Sharpe 1982) has shown that the temperature of the Bushveld magma was between 1200 and 1300°C. On this basis, the overload pressure at the time of emplacement of the marginal zone was between 1.1 and 2.4 kbars (hatched field in Fig. 9), and the overload pressure of the critical zone magma was between 0.6 and 1.6 kbars (dotted field in Fig. 9). Because merwinite and periclase are absent in xenoliths in the marginal zone, we conclude that the gabbronoritic magma of the marginal zone had a lower temperature than the feldspathic pyroxenitic magma of the critical zone. Assuming a temperature of 1200°C for the marginal zone magma and 1300°C for the critical zone magma, the pressure estimates overlap in the range 1.1 to 1.6 kbars.

Two different kind of textures are predominant: a granoblastic-polygonal texture caused by prograde metamorphism, and a symplectitic intergrowth caused by retrograde metamorphism. In granoblastic-polygonal textures, olivine, monticellite, and spinel are markedly closer to end-member compositions, and the $Fe^{3+}/Fe^{2+}$ value in spinel is much higher, than in the symplectites.

Calc-silicate xenoliths in the Bushveld Complex record a series of irreversible reactions that took place during devolatilization of the original carbonates. Therefore, the maximum *P–T* conditions are potentially frozen in and can be calculated provided that the reactions that occurred can be properly characterized. An internally consistent set of thermodynamic data has been compiled and used

to establish equilibrium conditions of xenoliths included in the marginal and critical zones. Xenoliths near the floor have lower maximum temperatures of equilibration than the xenoliths in the critical zone.

## ACKNOWLEDGEMENTS

The authors are grateful to W.E. Trzcienski, Jr., J.L. Jambor, R.F. Martin and an anonymous referee for critical reading of the manuscript, which was considerably improved by their remarks. Thanks are also due to G. von Gruenewaldt and the Council for Scientific and Industrial Research (C.S.I.R.), who made this project possible. The authors are indebted to H. Horsch for her assistance in the microprobe work.

## REFERENCES

ADAMS, G.E. & BISHOP, F.C. (1985): An experimental investigation of thermodynamic mixing properties and unit-cell parameters of forsterite–monticellite solid solutions. *Am. Mineral.* **70**, 714-722.

BOWEN, N.L. (1940): Progressive metamorphism of siliceous limestones and dolomite. *J. Geol.* **48**, 225-274.

BROUSSE, C., NEWTON, R.C. & KLEPPA, O.J. (1984): Enthalpy of formation of forsterite, enstatite, akermanite, monticellite and merwinite at 1073 K determined by alkali borate solution calorimetry. *Geochim. Cosmochim. Acta* **48**, 1081-1088.

BURNHAM, C.W. (1979): Magmas and hydrothermal fluids. *In* Geochemistry of Hydrothermal Ore Deposits (H.L. Barnes, ed.). John Wiley & Sons, New York (71-136).

CHARLU, T.V., NEWTON, R.C. & KLEPPA, O.J. (1981): Thermochemistry of synthetic $Ca_2Al_2SiO_7$ (gehlenite) – $Ca_2MgSi_2O_7$ (akermanite) melilites. *Geochim. Cosmochim. Acta* **45**, 1609-1617.

DEER, W.A., HOWIE, R.A. & ZUSSMAN, J. (1975): *An Introduction to the Rock-Forming Minerals.* Longman, London.

DE SANTIS, R., BREEDVELD, G.J.F. & PRAUSNITZ, J.M. (1974): Thermodynamic properties of aqueous gas mixtures at advanced pressures. *Ind. Eng. Chem. Process Des. Dev.* **13**, 374-377.

ENGLAND, P.C. & THOMPSON, A.B. (1984): Pressure–temperature–time paths of regional metamorphism. I. Heat transfer during the evolution of regions of thickened continental crust. *J. Petrol.* **25**, 894-928.

FINGER, L.W. (1972): The uncertainty in the calculated ferric iron content of a microprobe analysis. *Carnegie Inst. Washington Year Book* **71**, 600-603.

FLOWERS, G.C. (1979): Correction of Holloway's (1977) adaptation of the modified Redlich–Kwong equation of state for calculation of fugacities of molecular species in supercritical fluids of geologic interest. *Contrib. Mineral. Petrol.* **69**, 315-318.

FYFE, W.S., PRICE, N.J. & THOMPSON, A.B. (1978): *Fluids in the Earth's Crust. Their Significance in Metamorphic, Tectonic and Chemical Transport.* Elsevier, Amsterdam, The Netherlands.

GUO, Q. (1984): Topological relations in multisystems of more than $n+3$ phases. *J. Metamorph. Geol.* **2**, 267-295.

HELGESON, H.C., DELANY, J.M., NESBITT, H.W. & BIRD, D.K. (1978): Summary and critique of the thermodynamic properties of rock-forming minerals. *Am. J. Sci.* **278A.**

HEMINGWAY, B.S., EVANS, H.T., JR., NORD, G.L., JR., HASELTON, H.T., JR., ROBIE, R.A. & MCGEE, J.J. (1986): Åkermanite: phase transitions in heat capacity and thermal expansion, and revised thermodynamic data. *Can. Mineral.* **24**, 425-434.

HOLLAND, T.J.B. & POWELL, R. (1985): An internally consistent thermodynamic dataset with uncertainties and correlations. 2. Data and results. *J. Metamorph. Geol.* **3**, 343-370.

IRVINE, T.N. & SHARPE, M.R. (1982): Source-rock compositions and depth of origin of Bushveld and Stillwater magmas. *Carnegie Inst. Washington Year Book* **81**, 294-303.

JOUBERT, J. (1976): *Gemetamorfoseerde karbonaatinsluitsels in die bosone van die Bosveldstollingskompleks, wes van Roossenekal, Transvaal.* M.Sc. thesis, Univ. Pretoria, Hillcrest, South Africa.

KERRICK, D.M. & JACOBS, G.K. (1981): A modified Redlich–Kwong equation for $H_2O$, $CO_2$ and $H_2O$–$CO_2$ mixtures at elevated pressures and temperatures. *Am. J. Sci.* **281**, 735-767.

MOSTERT, A.B. (1982): The mineralogy, petrology and sulphide mineralization of the Platreef north-west of Potgietersrus, Transvaal, Republic of South Africa. *Geol. Surv. S. Afr. Bull.* **72**, 1-48.

OLESCH, M. (1975): Synthesis and solid solubility of trioctahedral brittle micas in the system CaO–MgO–$Al_2O_3$–$SiO_2$–$H_2O$. *Am. Mineral.* **60**, 188-199.

PAGE, D.C. (1970): *The Mineralogy of South African Jade and the Associated Rocks in the District Rustenburg, Western Transvaal.* M.Sc. thesis, Univ. Pretoria, Hillcrest, South Africa.

PHILPOTTS, A.R., PATTISON, E.F. & FOX, J.S. (1967): Kalsilite, diopside and melilite in a sedimentary xenolith from Brome Mountain, Quebec. *Nature* **214**, 1322-1323.

POWELL, R. & HOLLAND, T.J.B. (1985): An internally consistent thermodynamic dataset with uncertainties and correlations. 1. Methods and a worked example. *J. Metamorph. Geol.* **3**, 327-342.

ROBIE, R.A., HEMINGWAY, B.S. & FISHER, J.R. (1978): Thermodynamic properties of minerals and related

substances at 298.15 K and 1 bar ($10^5$ pascals) pressure and at higher temperatures. *U.S. Geol. Surv., Bull.* **1452.**

ROEDDER, E. (1984): Fluid inclusions. *Mineral. Soc. Am., Rev. Mineral.* **12.**

ROSEBOOM, E.H., JR. & ZEN, E-An (1982): Unary and binary multisystems, topological classification of phase diagrams and relation to Euler's theorem on polyhedra. *Am. J. Sci.* **282,** 286-310.

SAXENA, S.K. (1973): *Thermodynamics of Rock-Forming Crystalline Solutions.* Springer Verlag, New York.

SHARP, Z.D., ESSENE, E.J., ANOVITZ, L. M., METZ, G.W., WESTRUM, E.F., JR., HEMINGWAY, B.S. & VALLEY, J.W. (1986): The heat capacity of a natural monticellite and phase equilibria in the system CaO–MgO–$SiO_2$–$CO_2$. *Geochim. Cosmochim. Acta* **50,** 1475-1484.

SHMULOVICH, K.I. (1969): About stability of merwinite in the system CaO–MgO–$SiO_2$–$CO_2$. *Dokl. Akad. Nauk USSR* **184,** 1177-1179 (In Russian).

SKINNER, B.J. (1966): Thermal expansion. *In* Handbook of Physical Constants (S.P. Clark, Jr. ed.). *Geol. Soc. Am. Mem.* **97.**

TRACY, R.J. (1978): Monticellite marble at Cascade Mountain, Adirondack Mountains, New York. *Am. Mineral.* **63,** 991-999.

VALLEY, J.W. & ESSENE, E.J. (1980): Akermanite in the Cascade Slide xenolith and its significance for regional metamorphism in the Adirondacks. *Contrib. Mineral. Petrol.* **74,** 143-152.

WALTER, L.S. (1963): Experimental studies on Bowen's decarbonation series. I. *P-T* univariant equilibria of the "monticellite" and "akermanite" reactions. *Am. J. Sci.* **261,** 488-500.

WANG, H.F. (1978): Elastic constant systematics. *Phys. Chem. Miner.* **3,** 251-261.

WILLEMSE, J. & BENSCH, J.J. (1964): Inclusions of original carbonate rocks in gabbro and norite of the eastern part of the Bushveld Complex. *Trans. Geol. Soc. S. Afr.* **67,** 1-87.

YODER, H.S., JR. (1968): Akermanite and related melilite-bearing assemblages. *Carnegie Inst. Washington Year Book* **66,** 471-477.

_____ & EUGSTER, H.P. (1955): Synthetic and natural muscovites. *Geochim. Cosmochim. Acta* **8,** 225-280.

YOSHII, M. & MAEDA, K. (1975): Relations between barium content and the physical and optical properties in the manganoan phlogopite – kinoshitalite series. *Mineral. J.* **8,** 58-65.

ZEN, E-AN (1966): Construction of pressure–temperature diagrams for multicomponent systems after the method of Schreinemakers – a geometric approach. *U.S. Geol. Surv. Bull.* **1225.**

ZHARIKOV, V.A., SHMULOVICH, K.I. & BULATOV, V.K. (1977): Experimental studies in the system CaO–MgO–$Al_2O_3$–$SiO_2$–$CO_2$–$H_2O$ and conditions of high temperature metamorphism. *Tectonophysics* **43,** 145-162.

*Received October 2, 1987, revised manuscript accepted December 3, 1988.*

## APPENDIX: MIXING BEHAVIOR OF THE FLUID PHASE

For the thermodynamic calculations of reaction equilibria involving a fluid phase consisting of $H_2O$ and $CO_2$, it is necessary to calculate $f(H_2O)$ and $f(CO_2)$ at different $P$ and $T$. There are various models explaining the behavior of the fluid phase. Kerrick & Jacobs (1981) applied a nonideal mixing model for $H_2O$ and $CO_2$ at $T < 800°C$ ($P > 1$ kbar) and assumed ideal mixing at higher temperatures. De Santis *et al.* (1974) and Flowers (1979) preferred a nonideal mixing model for $H_2O$ and $CO_2$ even at highly elevated $T$. They considered a positive deviation from ideality at $T < 650°C$ and a negative deviation from ideality at higher $T$. The latter behavior is due to the complex-forming reaction of water and carbon dioxide ($H_2O + CO_2 = H_2CO_3$). The $T$ of high-grade reactions involving a $CO_2$–$H_2O$ mixture are therefore lower than with a model of ideal mixing, especially at highly elevated $T$. Experimental results by Zharikov *et al.* (1977) provide evidence that the negative deviation from ideality, assumed by de Santis *et al.* (1974) and Flowers (1979), is still not sufficient. These experiments involved calcite, forsterite, diopside, åkermanite, monticellite, merwinite and periclase at $T > 700°C$ and $P = 1$ kbar. Zharikov *et al.* (1977) compared their results with others (Walter 1963, Shmulovich 1969) and with calculations based on those experiments. All of the above authors ascertained reaction temperatures for low mole fractions of carbon dioxide, which are even lower than those calculated by de Santis *et al.* (1974) and Flowers (1979). It can be assumed that the negative deviation from ideality is due to further complex-forming reactions, in which a mineral phase participates. The most likely participant in high-temperature reactions involving calc-silicates is calcite (*e.g.:* $CaCO_3 + CO_2 + H_2O = CaH_2[CO_3]_2$). The excess energy of reaction for $H_2O$ and $CO_2$, respectively, is most probably due to complex-forming reactions involving calcite at $T > 700°C$.

In a first approach the following equation is used to evaluate this excess free energy:

$$G^{ex}(\text{cal}) \cong [(51.0 - 0.053 * T) * X^2] / 0.004184,$$

where $T$ is the temperature in K, the mole fraction $X$ refers to $H_2O$ in decarbonation reactions and $CO_2$ in dehydration reactions. This equation is derived from the experimental work from Zharikov *et al.* (1977) and produces an even higher positive deviation from ideality than described by the modified Redlich–Kwong equation (Flowers 1979). Until experimental results on complex-forming reactions between fluids and minerals at $T > 700°C$ and $P$ in the appropriate range are available, we have to use this empirical "make fit" factor.